




Article

Parametric Study and Investigations of Bead Geometries of GMAW-Based Wire–Arc Additive Manufacturing of 316L Stainless Steels

Rakesh Chaudhari , Heet Parmar, Jay Vora * and Vivek K. Patel 

Department of Mechanical Engineering, School of Technology, Pandit Deendayal Energy University, Raisan, Gandhinagar 382007, India; rakesh.chaudhari@sot.pdpu.ac.in (R.C.); heet.pmtmm20@sot.pdpu.ac.in (H.P.); vivekp@sot.pdpu.ac.in (V.K.P.)

* Correspondence: jay.vora@sot.pdpu.ac.in

Abstract: Appropriate selection of wire–arc additive manufacturing (WAAM) variables imparts bead geometries with characteristics of multi-layer structures. Thus, the present study aimed to optimize the gas metal arc welding (GMAW)-based WAAM variables of travel speed (TS), wire feed speed (WFS), and voltage (V) for the bead geometries of bead width (BW) and bead height (BH) on an SS 316L substrate. Single-layer depositions were made through a metallic wire of SS 316L by following an experimental matrix of the Box–Behnken design (BBD) technique. Multivariable regression equations were generated for design variables and responses, and ANOVA was used to investigate the feasibility of the obtained regression equations. WFS was the highest contributor affecting the BW, followed by V and TS, while WFS was again the highest contributor affecting the BH, followed by TS and V. Heat transfer search (HTS) optimization was used to attain optimal combinations. The single-objective optimization result showed a maximum bead height and minimum bead width of 6.72 mm and 3.72 mm, respectively. A multi-layer structure was then fabricated by considering an optimization case study, and it showed optimized parameters at a WFS of 5.50 m/min, TS of 141 mm/min, and voltage of 19 V with the bead height and bead width of 5.01 mm and 7.81 mm, respectively. The multi-layered structure obtained at the optimized parameter was found to be free from disbonding, and seamless fusion was detected between the obtained layers of the structure. The authors believe that the present study will be beneficial for industrial applications for the fabrication of multi-layer structures.

Keywords: wire–arc additive manufacturing (WAAM); gas metal arc welding (GMAW); optimization; 316L stainless steels; multi-layer structures; bead geometries



Citation: Chaudhari, R.; Parmar, H.; Vora, J.; Patel, V.K. Parametric Study and Investigations of Bead Geometries of GMAW-Based Wire–Arc Additive Manufacturing of 316L Stainless Steels. *Metals* **2022**, *12*, 1232. <https://doi.org/10.3390/met12071232>

Academic Editor: Dmitry A. Chinakhov

Received: 28 June 2022

Accepted: 18 July 2022

Published: 21 July 2022

Publisher's Note: MDPI stays neutral with regard to jurisdictional claims in published maps and institutional affiliations.



Copyright: © 2022 by the authors. Licensee MDPI, Basel, Switzerland. This article is an open access article distributed under the terms and conditions of the Creative Commons Attribution (CC BY) license (<https://creativecommons.org/licenses/by/4.0/>).

1. Introduction

Currently, the additive manufacturing (AM) process is an extensively preferred technique for the development of objectively difficult structures without the use of a mold as it widely expands the manufacturing capability and resilience [1,2]. The fabrication and formation of complex three-dimensional (3D) parts are converted into the step-by-step inclusion of lean component layers governed by an automated model using AM techniques [3]. Heat sources used in the AM of solid structures consist of electric arcs, laser beams, and electron beams. The energy charge is compact and the structural behavior is comparably accurate during the heat source of laser and electron beams [4]. These two heat source processes of laser and electron beams utilize direct energy deposition and powder bed fusion techniques [5,6]. Therefore, metal powder as feedstock is essential for these techniques, which in turn limits their production efficiency [7]. Due to this reason, the production cost of the process increases by limiting the use of laser and electron beams in the fabrication of extensive metallic structures on a larger scale [8]. Electric arc as a heat source is a promising technique for the fabrication of large-scale intricate metallic structures owing to their high rate of deposition, reduced cost, and minimal wastage rate [9,10]. A

metal wire is employed as feedstock material in the electric arc method, and its cost relative to metal power for equal weight is very low [11]. Therefore, the WAAM technique using an electric arc is more suitable than laser and electron beam techniques. Gas metal arc welding (GMAW)-based WAAM is widely preferred due to its capability of fabricating thin multi-layer structures with a lower capital cost, ease of material deposition, and high deposition rate [12,13]. However, several challenges arise during the WAAM of metallic structures such as post-processing techniques, reduced surface quality, surface morphology, changes in microstructure, and mechanical properties. This requires additional machining to be performed. Due to the lower wastage of material during WAAM, the entire process still remains economical in comparison with subtractive machining processes [14]. Appropriate selection of WAAM variables imparts bead geometries with characteristics of multi-layer structures [15,16].

The features of the weld geometry and dimensional precision were both affected by the process parameters of WAAM. Construction of a single-layered geometry determines the dimensional precision which is evaluated by its homogeneity and stability [17]. As a result, suitable design variables to achieve a specified component accuracy are essential and critical for WAAM. Incorrect selection of design variables will result in eminent issues such as partial fusing, hump, and porosity [18]. Parts with serious flaws will have their mechanical characteristics drastically reduced. Furthermore, past studies often employed design variables that were selected from a specified range [19]. As a result, adjustment of processing parameters that impact weld bead geometry and quality in the construction of multi-walled components needs to be considered. Thus, it is essential to optimize the design variables of the WAAM process. Optimized parameters give a good quality of properties to the final components. The heat transfer search (HTS) technique was successfully implemented for various manufacturing systems [20–22].

Kumar et al. [23] carried out a parametric study of the GMAW-based WAAM process to manufacture steel structures by employing a copper-coated steel wire. Single-layer deposition was performed by considering the design variables of travel speed (TS), voltage (V), gas flow rate, and current. Bead height (BH) and bead width (BW) were selected as response variables. TS was observed as the highest contributor followed by voltage affecting the BW response with the involvement of 52.29% and 17.08%, respectively. TS followed by voltage was again observed to be the highest contributor affecting the BH response with the involvement of 43% and 15.81%, respectively. For selected responses, the desirability function was utilized as an optimization process. A multi-layer structure was successfully fabricated at optimal combinations of WAAM variables. Dinovitzer et al. [4] explored the impact of the design variables of WAAM on manufacturing components on an SS 304 substrate by using a metallic wire of Hastelloy X. Taguchi's technique along with ANOVA was implemented to evaluate the impact of the design variables. Current and TS were observed as the highest contributors affecting the responses. Another study reported by Xiong et al. [12] explored the impact of GMAW-based WAAM design variables on surface quality. It was observed that lower wire feed speed (WFS) improved the surface quality of the multi-layer structure. A study pertaining to the parametric optimization of the WAAM technique was carried out by Zhao et al. [19] for the enhancement and better quality of weld bead geometries. Geometrical features of the weld bead structure of the WAAM process are largely dependent on the selection of design variables and their appropriate values. Yuan et al. [24] established a parabola model to acquire the favorable path geometry and suitable process parameters of the WAAM technique. They concluded that the minimum values of WFS and TS will lead to a higher rate of production. As per the study reported by Kannan and Murugan [25] and Teixeira et al. [26], a higher deposition rate with simultaneous dimensional accuracy is largely dependent on the geometric structure of fabricated parts. Cadiou et al. [27] presented a 3D numerical model of WAAM to acquire the shape of the component as well as its temperature field. In the event of pulsed currents, this model tries to replicate the formation of a 304 SS rod beginning with operational variables. The geometry of the component was predicted by

modeling the detachment of deposited metal droplets. Mai et al. [16] optimized the design variables (current, voltage, and TS) of GMAW-based WAAM for the weld bead geometry of 308L steel. Experimental results show that the required geometry of weld bead was successfully fabricated at optimized parameters. Voltage was observed as the highest contributor followed by TS affecting the BW response with the involvement of 70.18% and 18.54%, respectively. TS followed by the current was observed to be the highest contributor affecting the BH response with the involvement of 48.11% and 38.27%, respectively. The fabricated structure at optimized conditions at a current of 122 A, TS of 368 mm/min, and voltage of 20 V was found to be without the presence of cracks. This shows the suitability of the proper selection of parameters for bead geometries and surface quality. Vora et al. [28] employed a metaheuristic TLBO algorithm for optimizing the design variables of the GMAW-based WAAM technique to acquire better geometrical weld beads for multi-layer structures. They used 2.25Cr-1.0Mo as a substrate with a metal-cored wire as feedstock. Optimization results yielded successful fabrication of a thin multi-layered structure with the optimal BW of 7 mm and BH of 6.07 mm with the optimal parameter settings as follows: TS of 476 mm/min, voltage of 18 V, and WFS of 5.9 m/min. The multi-layered structure obtained at optimized parameters was found to be free from disbonding, and seamless fusion was detected between the obtained layers of the structure. Thus, the literature demonstrated the necessity of a parametric study for obtaining the desired quality of the multi-layered structure.

The austenitic stainless steel 316L (SS316L) was created over three decades ago for use in fast breeder reactors [29]. SS 316L is an austenitic stainless-steel grade having a lower carbon content of 0.03% by wt. It is utilized in various industrial applications including marine and offshore applications, biomedical equipment, automobiles, petrochemical facilities, and nuclear reactors owing to its excellent characteristics of superior corrosion resistance, good weldability, high strength and ductility, strong biocompatibility, and comparatively cheap cost [30–32]. Studies pertaining to the parametric study of the weld bead geometries of the GMAW-based WAAM process have not been conducted appropriately on SS 316L substrates. The current study focused on the WAAM of 316L stainless steel. As per the studied literature, parametric studies on bead geometries for multi-layer structures employing the GMAW-based WAAM multi-layer structure of SS 316L have not been comprehensively reported. In the current study, we built an experimental platform and then performed WAAM with 316L stainless steel on it with optimized parameters.

In the present study, GMAW-based WAAM was employed to perform bead-on-plate trials on an SS 316L substrate by considering the TS, WFS, and V as design variables, while BH and BW were considered as responses. Multivariable regression equations were generated through results generated from the experimental matrix followed by the BBD approach of RSM. Analysis of variance (ANOVA) was used to investigate the feasibility of the regression equations. The HTS algorithm was employed to obtain the optimal combinations of design variables by considering single- and multi-objective optimization of BH and BW. A multi-layer structure was then fabricated by WAAM at the optimized process parameters. The authors believe that the present study will be beneficial for industrial applications for the fabrication of multi-layer structures.

2. Materials and Methods

2.1. Experimental Setup and Plan

KEMPPI PRO MIG-530 GMAW (Kemppei, Chennai, India) setup was employed in the present study for single-layer deposition on a 316L stainless steel substrate. Figure 1 shows the experimental setup used in the current study. Single-layer depositions were prepared through a metallic wire of SS 316L having a diameter of 1.2 mm on a 316L substrate. Table 1 depicts the chemical composition of the substrate and filler wire. Shielding gas with 98% Ar and 2% O₂ was employed for the deposition. In the existing experimental setup, the computer interface was used for CNC code programming to give input to the controller. The special purpose machine (SPM) enables the movement of the deposition torch on the

3 axes x, y, and z-axis. Shielding gas was delivered through the setup before the start of the program to prevent the mixing of ambient gases with the deposited material. The substrate was clamped on a work table, and the material was deposited by using a torch that can travel in any direction. The torch was raised to a predetermined height for the metal deposition. A thermocouple was inserted between the base plate and the HAZ zone to detect temperature.

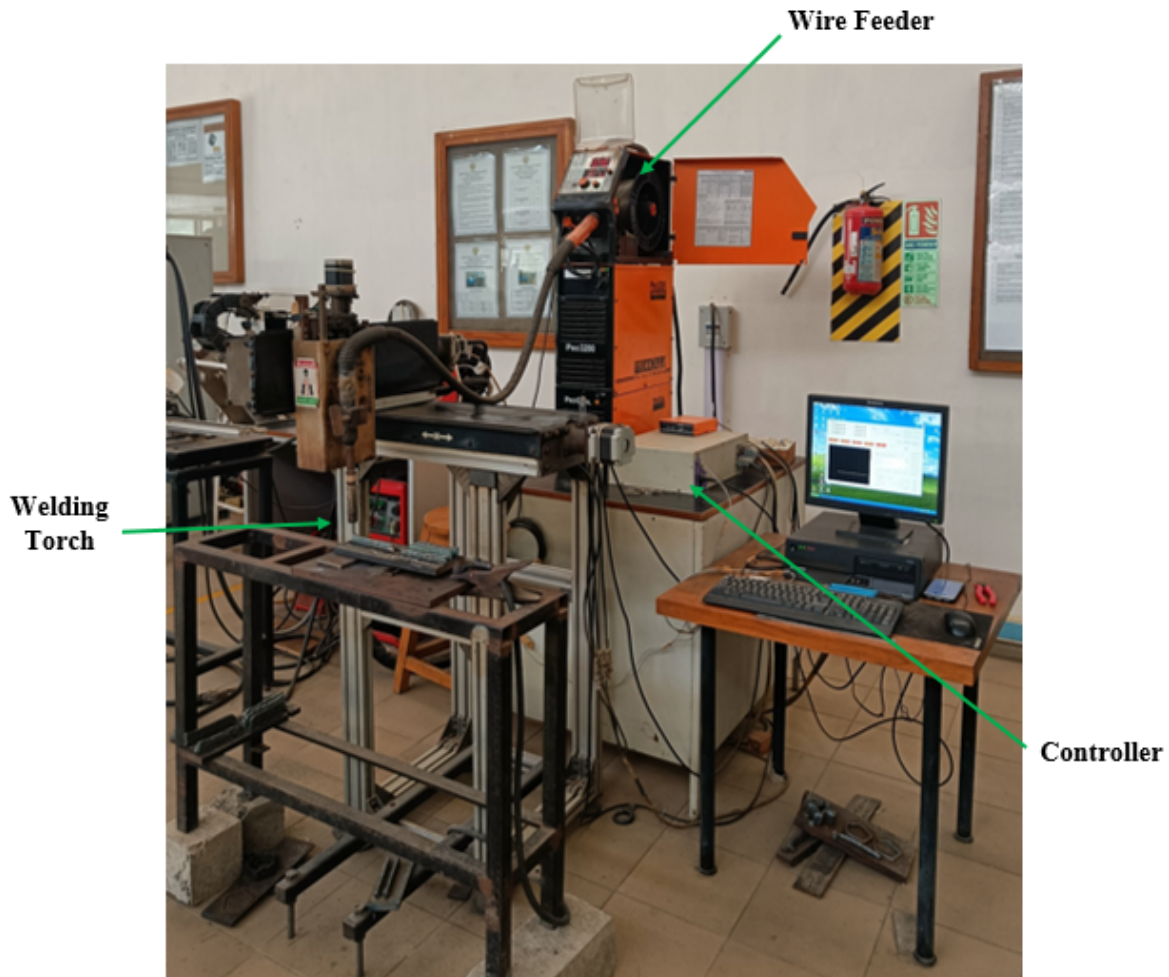


Figure 1. Experimental setup of WAAM process.

Table 1. Chemical composition substrate and metallic wire (SS 316L) [8].

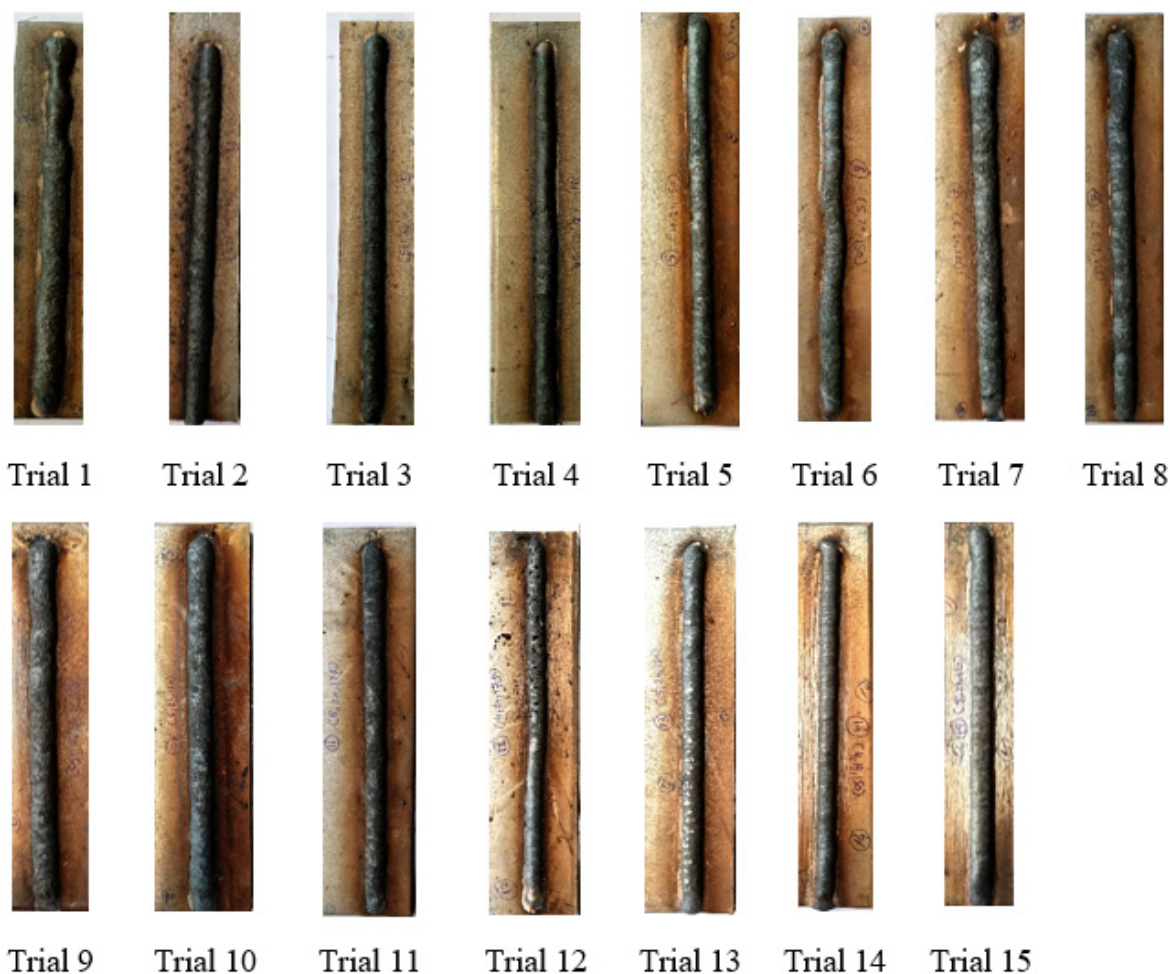
Element	Cr	Ni	Mo	Mn	Si	C	P	S	N	Fe
Substrate Plate	17.09	10.61	2.38	1.17	0.59	0.013	0.011	0.011	0.09	Balance
Metallic wire	17.09	10.61	2.38	1.17	0.59	0.013	0.011	0.011	0.09	Balance

Single-layer depositions were made through a metallic wire of SS 316L by following an experimental matrix of the BBD technique. On the basis of device capability and the past studied literature, WFS, TS, and voltage were selected as design variables. The range of these selected WAAM variables was decided by performing some pilot experiments. A constant deposition length of 190 mm, length of the arc of 3 mm, and gas flow rate of 15 L/min were considered throughout the single-layer deposition. The effect of the selected WAAM variables was studied on weld bead geometries (BW and BH). Table 2 displays the experimental conditions of the GMAW-based WAAM process.

Table 2. Design variables used in present study with their value/range.

Design Variable	Unit	Value/Range
WFS	m/min	4; 5; 6
TS	mm/min	125; 150; 175
Voltage	V	19; 20; 21
Arc length	mm	3
Gas flow rate	L/min	15
Weld bead length	mm	190

By properly arranging the experimental matrix, Box and Behnken utilizes the RSM approach to obtain an optimum response. BBD decreases the total number of experimental trials by saving both money and time [33]. Furthermore, the BBD approach creates a correlation between machining factors and responses [34]. The selected WAAM process parameters were varied at 3 levels, and a total of 15 runs were completed as shown in Figure 2 followed by an experimental matrix of the BBD. The effect of the selected factors was investigated on BW and BH. Each single-layer deposition was cut into cross-sections for the measurement of response variables. Optical microscopy was employed to determine the response measures of BH and BW. The average value of three repetitions was considered for investigations. Figure 3 displays the measurement method for the determination of BW and BH employed in the current study.

**Figure 2.** Single-layered deposition on 316L substrate.

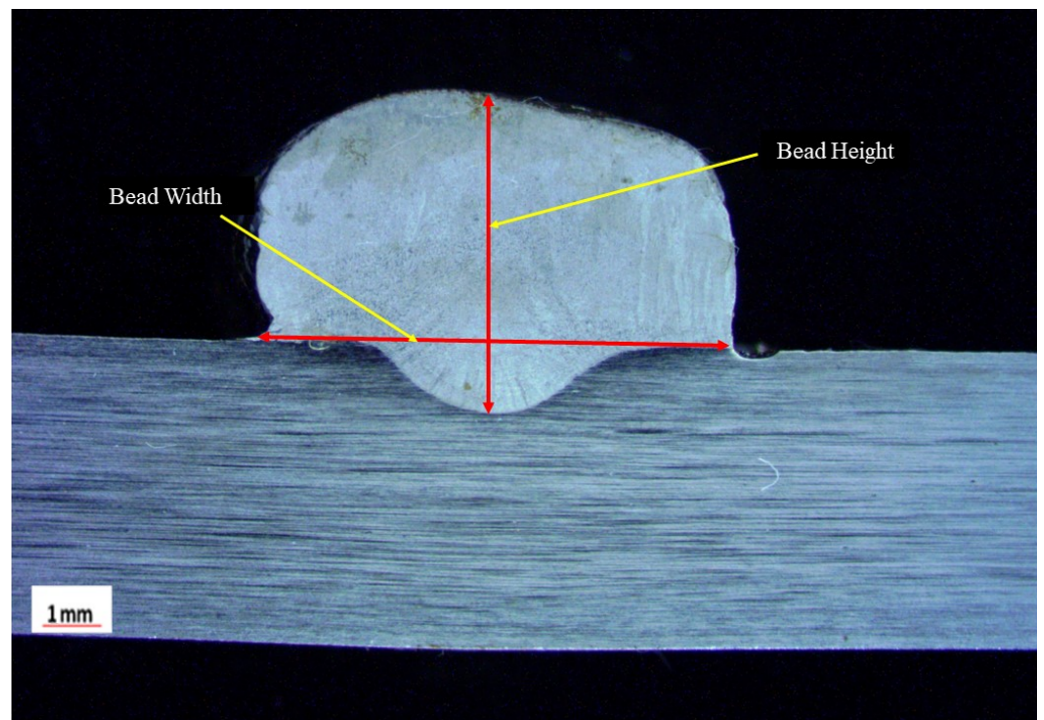


Figure 3. Measurement process of bead geometries.

2.2. Optimization by HTS Algorithm

Vivek and Savsani [35] developed an HTS algorithm that operates on the principle of heat transfer (HT) among the system particles and surroundings which tries to obtain thermal equilibrium. It utilizes the three mediums of HT (conduction, convection, and radiation) to acquire an equilibrium condition. Each HT medium receives equal opportunities, and the algorithm randomly selects any one of the mediums. Thus, HTS starts with a primary arbitrarily produced population. It consists of population size (particles) and design variables. Every generation subsequently modifies the population size by arbitrarily picking the mode of HT. This process is repeated, and the system accepts a solution with good functional value and subsequently replaces poor solutions from the system with elite solutions [36]. The step-by-step methodology of the HTS technique is depicted in Figure 4.

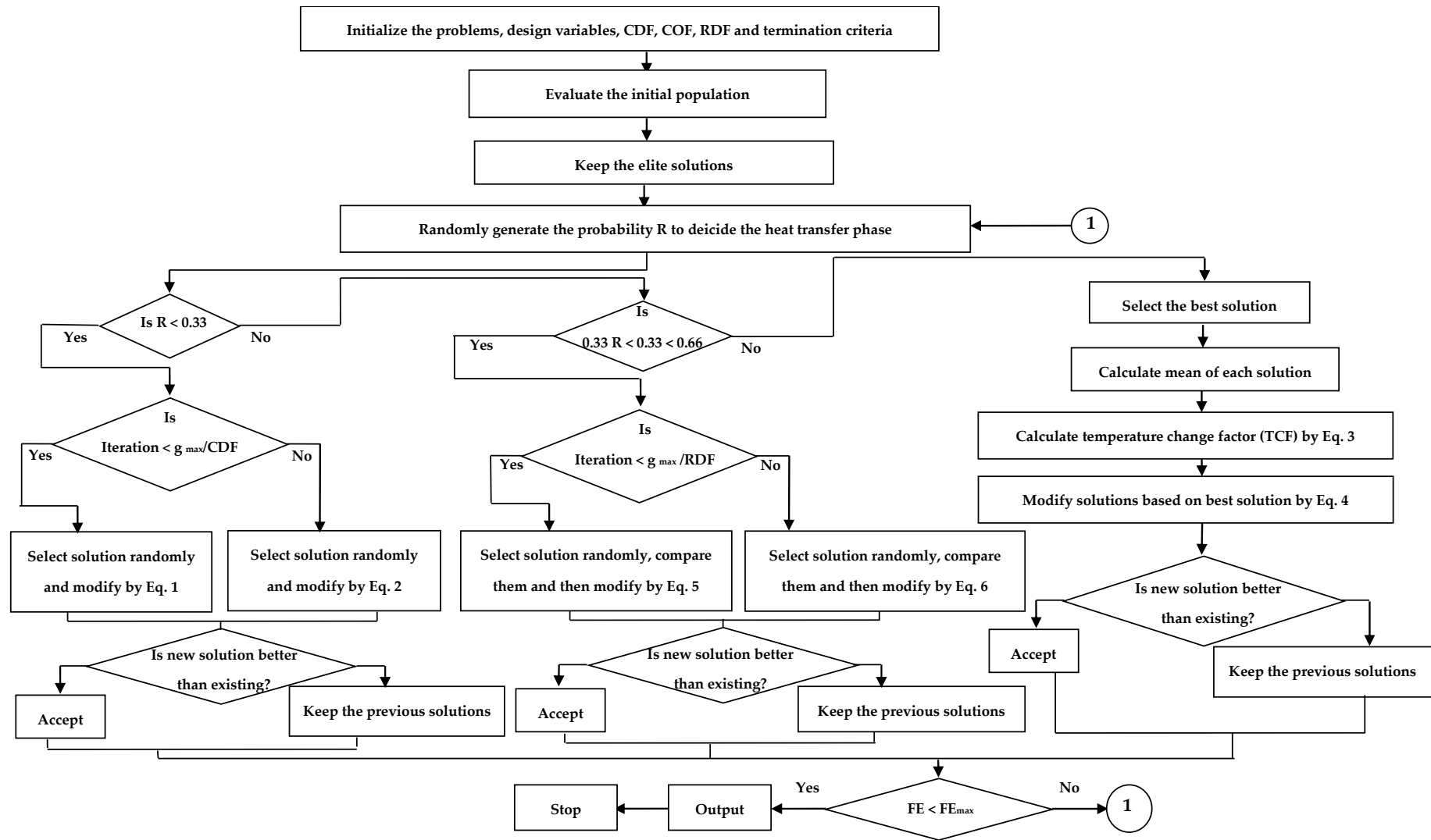


Figure 4. HTS algorithm methodology [37].

2.2.1. HT by Conduction

The solutions from the systems are improved from the conduction HT medium by using Equations (1) and (2).

$$X'_{j,i} = \begin{cases} X_{k,i} + (-R^2 X_{k,i}), & \text{iff}(X_j) > f(X_k) \\ X_{j,i} + (-R^2 X_{j,i}), & \text{iff}(X_j) < f(X_k) \end{cases}; \text{if } g \leq g_{max}/CDF \quad (1)$$

$$X'_{j,i} = \begin{cases} X_{k,i} + (-r_i X_{k,i}), & \text{iff}(X_j) > f(X_k) \\ X_{j,i} + (-r_i X_{j,i}), & \text{iff}(X_j) < f(X_k) \end{cases}; \text{if } g > g_{max}/CDF \quad (2)$$

2.2.2. HT by Convection

The solutions from the systems are improved from the convection HT medium by using Equations (3) and (4).

$$X'_{j,i} = X_{j,i} + R \times (X_s - X_{ms} \times TCF) \quad (3)$$

$$TCF = \begin{cases} \text{abs}(R - r_i), & \text{if } g \leq g_{max}/COF \\ \text{round}(1 + r_i), & \text{if } g > g_{max}/COF \end{cases} \quad (4)$$

2.2.3. Heat Transfer by Radiation Mode

The solutions from the systems are improved from the radiation HT medium by using Equations (5) and (6).

$$X'_{j,i} = \begin{cases} X_{j,i} + R \times (X_{k,i} - X_{j,i}), & \text{iff}(X_j) > f(X_k) \\ X_{j,i} + R \times (X_{j,i} - X_{k,i}), & \text{iff}(X_j) < f(X_k) \end{cases}; \text{if } g \leq g_{max}/RDF \quad (5)$$

$$X'_{j,i} = \begin{cases} X_{j,i} + r_i \times (X_{k,i} - X_{j,i}), & \text{iff}(X_j) > f(X_k) \\ X_{j,i} + r_i \times (X_{j,i} - X_{k,i}), & \text{iff}(X_j) < f(X_k) \end{cases}; \text{if } g > g_{max}/RDF \quad (6)$$

3. Results and Discussions

Results of cross-sectional geometries were investigated by using the measured responses of BW and BH from optical microscopy. Table 3 displays the design variables by following an experimental matrix of the BBD technique along with the measured responses of BW and BH.

Table 3. Design variables of WAAM process with measured responses.

Std. Order	Run Order	WFS	TS	Voltage	BW	BH
6	1	6	150	19	9.24	5.82
1	2	4	125	20	6.89	4.23
10	3	5	175	19	6.23	4.27
12	4	5	175	21	8.68	5.12
7	5	4	150	21	7.38	4.11
14	6	5	150	20	7.53	4.61
2	7	6	125	20	9.88	6.05
9	8	5	125	19	8.28	5.3
15	9	5	150	20	7.46	4.55
8	10	6	150	21	9.97	5.89
4	11	6	175	20	9.17	5.62
3	12	4	175	20	5.9	3.63
13	13	5	150	20	7.41	4.51
5	14	4	150	19	6.25	3.99
11	15	5	125	21	8.47	5.21

3.1. Regression Equations for BW and BH

Non-linear regression equations were generated to establish relationships among the WAAM design variables and responses (BH and BW) by integrating the RSM method through Minitab v17 software. The obtained regression equations were validated through ANOVA test results and residual plots. Regression models for BW and BH were depicted in Equations (7) and (8) by following a stepwise method.

$$BW = 201.1 - 2.278 \cdot x_1 - 0.4697 \cdot x_2 - 16.06 \cdot x_3 + 0.3758 \cdot x_1^2 + 0.3308 \cdot x_3^2 + 0.02260 \cdot x_2 \cdot x_3 \quad (7)$$

$$BH = 135.1 - 0.589 \cdot x_1 - 0.2824 \cdot x_2 - 11.06 \cdot x_3 + 0.1517 \cdot x_1^2 + 0.000279 \cdot x_2^2 + 0.2442 \cdot x_3^2 + 0.0094 \cdot x_2 \cdot x_3 \quad (8)$$

where x_1 represents the WFS, x_2 represents TS, and x_3 represents voltage.

3.2. ANOVA for BW and BH

The adequacy and acceptability of the obtained regression equations were validated through ANOVA test results. Minitab v17 was utilized for the evaluation of significant and non-significant model terms from ANOVA. A confidence level of 5% was selected to assess the significance. Thus, a probability value lower than 0.05 suggests an influential effect of the respective term on the response variables of bead width and bead height [38]. Table 4 displays the statistical analysis of bead width from ANOVA by following a stepwise approach to eliminate terms that do not contribute to the response. The statistical significance of the quadratic model for bead width displayed the significance of regression, linear, square, and interaction model terms. As per the confidence level of 5%, statistically significant factors include all the linear terms (WFS, TS, and V), the square terms of $WFS \times WFS$ and $TS \times TS$, and the interaction term of $TS \times V$. The large probability value of the lack of fit along with its non-significance specified the acceptability and fitness of the model for bead width [39]. Higher F-values specified that WFS was the highest contributor affecting the BW response followed by V and TS. An R^2 value adjacent to one suggests that the regressions predict the response value [40]. The model summary displayed in Table 4 depicts the least difference between R^2 values, and all of them are adjacent to one. Thus, the developed regression model for BW showed adequacy and acceptability through the validation results of the ANOVA test.

Table 4. ANOVA for bead width (BW).

Source	DF	SS	MS	F	P	Significance
Regression	6	23.7671	3.9612	130.10	0.000	*
Linear	3	21.6209	7.2070	236.71	0.000	*
WFS	1	17.5232	17.5232	575.555	0.000	*
TS	1	1.5665	1.5665	51.45	0.000	*
V	1	2.5312	2.5312	83.14	0.000	*
Square	2	0.8693	0.4247	14.28	0.002	*
WFS \times WFS	1	0.5245	0.5245	17.23	0.003	*
TS \times TS	1	0.4064	0.4064	13.35	0.006	*
Interaction	1	1.2769	1.2769	41.94	0.000	*
TS \times V	1	1.2769	1.2769	41.94	0.000	*
Error	8	0.2436	0.0304	-	-	
Lack of fit	6	0.2242	0.0374	3.85	0.22	#
Pure error	2	0.0194	0.0097	-	-	-
Total	14	24.0107	-	-	-	-

Model Summary: $R^2 = 98.99\%$; Adj. $R^2 = 98.22\%$; Pred. $R^2 = 95.52\%$. "*" represents significance, and "#" represents non-significance.

Statistical analysis of bead height response is represented in Table 5 by following a stepwise approach. The statistical significance of the quadratic model for bead height displayed the significance of regression, linear, square, and interaction model terms. Statistically significant factors include all the linear terms (WFS, TS, and V), all the square terms of $WFS \times WFS$, $TS \times TS$, and $V \times V$, and the interaction term of $TS \times V$. The large

probability value of the lack of fit along with its non-significance specified the acceptability and fitness of the model for bead width. Higher F-values specified that WFS was the highest contributor affecting the BH response followed by TS and V. The model summary displayed in Table 5 depicts the least difference between R^2 values, and all of them are adjacent to one. Thus, the developed regression model for BH showed adequacy and acceptability through the validation results of the ANOVA test.

Table 5. ANOVA for bead height (BH).

Source	DF	SS	MS	F	P	Significance
Regression	7	8.1587	1.1655	137.03	0.000	*
Linear	3	7.5726	2.5242	296.76	0.000	*
WFS	1	6.8821	6.8821	809.09	0.000	*
TS	1	0.5778	0.5778	67.93	0.000	*
V	1	0.1128	0.1128	13.26	0.008	*
Square	3	0.3651	0.1217	14.31	0.002	*
WFS × WFS	1	0.0849	0.0849	9.99	0.016	*
TS × TS	1	0.1120	0.1120	13.17	0.008	*
V × V	1	0.2201	0.2201	25.88	0.001	*
Interaction	1	0.2209	0.2209	25.97	0.001	*
TS × V	1	0.2209	0.2209	25.97	0.001	*
Error	7	0.5448	0.0085			
Lack of fit	5	0.0051	0.0109	4.30	0.199	#
Pure error	2	8.2182	0.0025			
Total	14					

Model Summary: $R^2 = 99.28\%$; Adj. $R^2 = 98.55\%$; Pred. $R^2 = 94.17\%$. “*” represents significance, and “#” represents non-significance.

3.3. Normal Probability Plot for Bead Width and Bead Height

Validation of the ANOVA test and its robustness can be effectively depicted by a normal probability plot of residuals. ANOVA test results are treated as effective and fit for the developed regression models if the normal probability plot of residuals fulfills the assumptions [41]. Thus, it is necessary to validate the results from the normal probability plot. Figure 5 represents the normal probability graph for bead width. All the residuals are placed in a straight line. This depicts the fitness of the developed regression models for bead width as it shows an absence of residual clustering with a normal scattering of all errors. A similar observation can be found in Figure 6 of the normal probability graph of bead height. Therefore, it can be concluded that all design variables of the present work signify a key role.

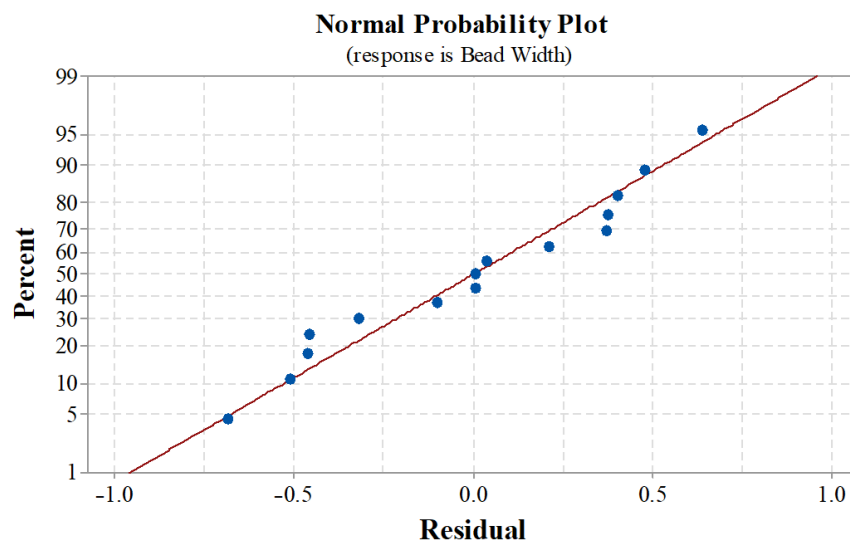


Figure 5. Normal probability plot for bead width.

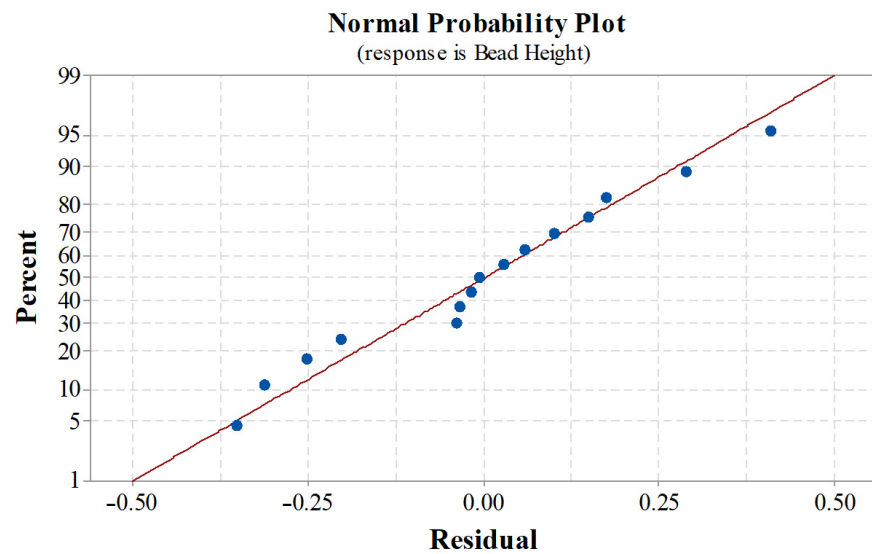


Figure 6. Normal probability plot for bead height.

3.4. Main Effect Plot for Bead Width and Bead Height

Figure 7 represents an effect of WAAM design variables (WFS, TS, and V) on bead width response. An increased value of WFS was observed to have a substantial effect on the bead width of the deposition. An enlarged speed of the metallic wire increases the deposition of material on the substrate [18]. Due to this reason, a negative effect on the increase in bead width was observed with an intensification in WFS. A plot of bead width vs. TS showed a positive effect of the increase in TS on bead width response. An increase in TS from 125 mm/min to 175 mm/min showed a drop in bead width. This was due to the higher speed of the torch at increased TS. With the increase in torch speed, there were fewer drops of molten metal being deposited, which resulted in a decrease in the bead width [23,42]. An increase in the value of voltage showed a negative impact on bead width owing to the widening of the arc. After increasing voltage, large droplets of molten metals were deposited which in turn increased the bead width of the deposition [43].

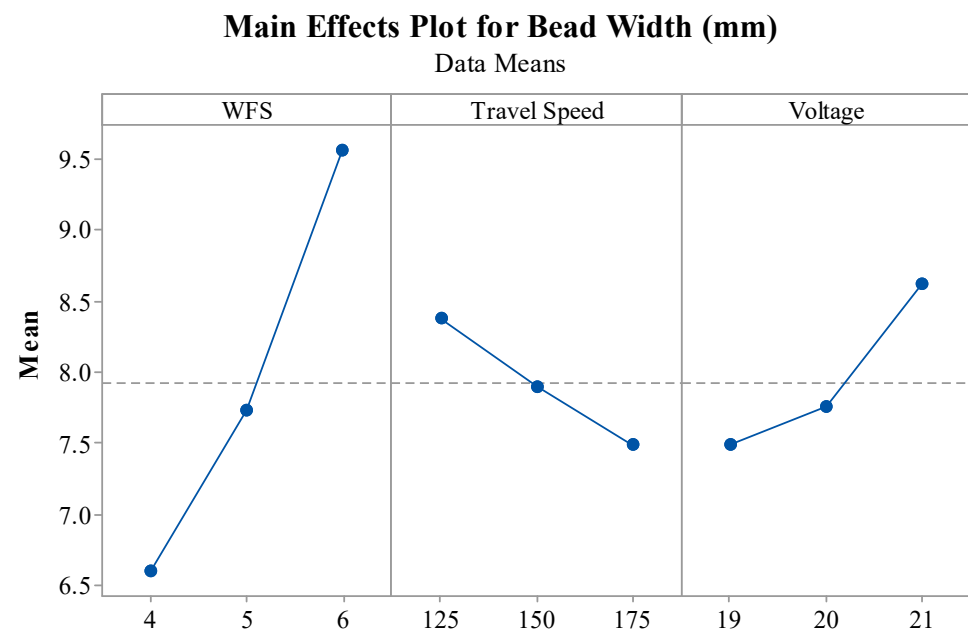


Figure 7. Main effect plot for bead width.

The influence of the WAAM design variables of WFS, TS, and V was studied on bead height response as shown in Figure 8. The bead height of the weld bead increases with the increase in material deposition due to the increased speed of the metallic wire coming from the nozzle [23,44]. The main reason behind this increased speed is the intensification in WFS. This can be observed from the plot of bead height vs. WFS wherein bead height was largely increased with an increase in WFS. The bead height of the single-layer deposition was observed to have a declined trend with an increase in TS from 125 mm/min to 175 mm/min. This was due to the higher speed of the torch at increased TS. A higher speed of the torch restricts the deposition of the material, and due to this reason, the bead height of the bead geometry decreases with an increase in TS [28,45]. The effect of voltage on bead height did not show any substantial effect as it was observed that bead height initially decreased with an increase in voltage from 19 to 20 V and then increased slightly with an increase in voltage from 20 to 21 V. However, the mean value of bead height was observed to be the same with very little variation. An appropriate value of these design variables can be obtained from parametric optimization.

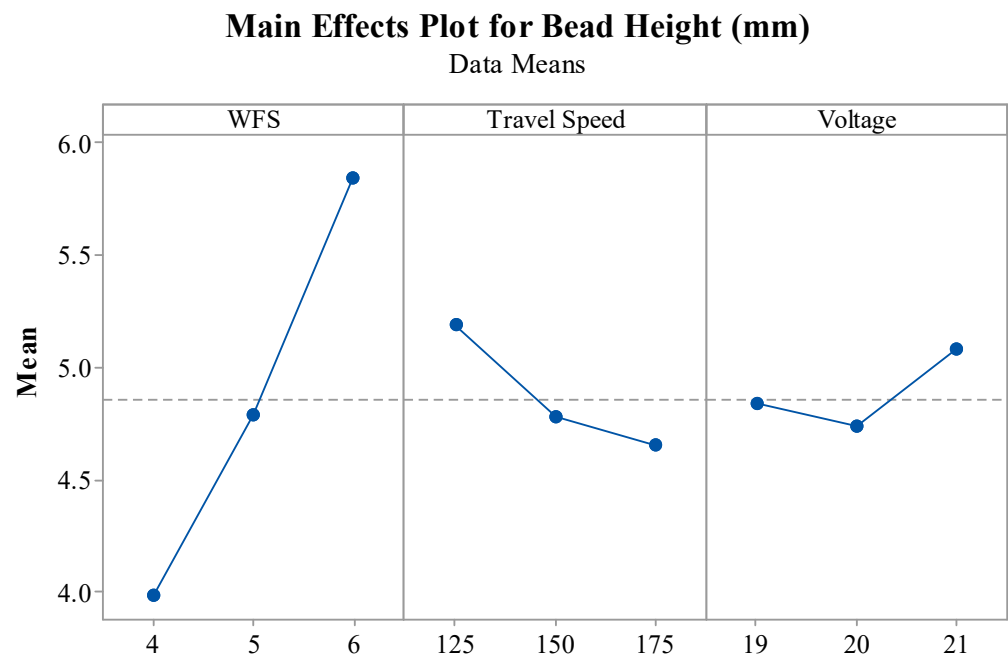


Figure 8. Main effect plot for bead height.

3.5. Optimization

The selected responses of bead height and bead width showed conflicting nature in correspondence with the levels of the design variables of WAAM. Thus, the HTS approach was used as an optimization technique for a set of optimal levels of both responses. For obtaining design variables suitable for multi-layer thin-walled structures, a higher bead height and lower bead width were considered during the implementation of HTS. The upper and lower bound levels of the design variables of WAAM were selected during the execution of the algorithm with the continuous values of WAAM variables. This includes the range of WFS from 4 m/min to 6 m/min, V from 19 V to 21 V, and TS from 125 mm/min to 175 mm/min. By considering the individual response of bead width and then bead height, their individual values were determined and are represented in Table 6 with percentage error. Least error between results achieved from HTS and validation resulted in good agreement between the bead geometry and WAAM variables.

Table 6. HTS results for individual response geometries.

Criteria	WAAM Variables			Predicted Results		Experimental Results	
	WFS	TS	V	BW	BH	BW	BH
Maximization of BH	6	125	19	10.21	6.43	9.96	6.72
Minimization of BW	4	175	19	3.57	5.22	3.43	5.47

However, the individual response suggested the opposing condition for the responses of bead width and bead height. Therefore, it becomes necessary to determine the optimal combination of design variables for both bead width and bead height. By considering the requirement of the fabrication of multi-layer thin-walled structures, 10 case studies were conducted as per Table 7. The objective function developed for these case studies is represented in Equation (9) which also considers the continuous values of WAAM variables.

$$\text{Obj} = w_1 \cdot (\text{BW}) + w_2 \cdot (\text{BH}) \quad (9)$$

where w_1 and w_2 represent the weights given during the HTS execution.

Table 7. Case study results for optimal solutions of bead geometries.

Weights		WAAM Variables			Bead Geometries	
BH	BW	WFS	TS	V	BH	BW
1	0	6	125	19	6.42	10.21
0.9	0.1	5.9	134	19	6.14	9.78
0.8	0.2	5.9	146	19	5.86	9.38
0.7	0.3	5.3	172	19	5.51	8.66
0.6	0.4	6	131	19	5.42	8.18
0.5	0.5	5.5	141	19	5.01	7.81
0.4	0.6	5.6	152	19	4.95	7.35
0.3	0.7	4	175	19	4.41	7.04
0.2	0.8	5	148	19	4.39	6.57
0.1	0.9	4.6	159	19	3.99	5.79
0	1	4	175	19	3.57	5.22

Depending upon the requirement of bead width and bead height dimensions, the user can select the appropriate combination of design variables shown in Table 7. All these case studies were validated by performing single-layer deposition trials. An error of less than 6% between the predicted results and actual results showed good agreement between the bead geometry and WAAM variables.

In addition to the ten case studies, Pareto fronts were also developed which provide non-dominated unique solutions. A total of 50 unique optimal solutions were generated with continuous values of WAAM variables by considering the different requirements of industrial applications. Table 8 shows unique solutions along with continuous values of WAAM variables, and Figure 9 depicts the Pareto graph of bead height vs. bead width. The user can select any optimal value as per their requirement of bead geometries for the fabrication of multi-layer thin-walled structures.

Table 8. Pareto optimal points.

Sr. No.	WFS	TS	V	Bead Height	Bead Width
1	4	175	19	3.57	5.23
2	6	125	19	6.43	10.20
3	5.3	173	19	4.65	6.89
4	5.2	174	19	4.54	6.68
5	4.1	175	19	3.63	5.30
6	4.9	173	19	4.27	6.27
7	4.8	175	19	4.16	6.05
8	5.5	127	19	5.78	9.10
9	6	169	19	5.47	8.43
10	5.4	128	19	5.64	8.88
11	6	128	19	6.33	10.08
12	5.8	172	19	5.20	7.88
13	5.9	175	19	5.30	7.97
14	5.9	128	19	6.21	9.86
15	4.4	173	19	3.85	5.66
16	5.7	125	19	6.07	9.57
17	5.7	127	19	6.01	9.49
18	5.5	171	19	4.87	7.33
19	5.5	175	19	4.85	7.17
20	5.4	125	19	5.74	9.00
21	5.9	159	19	5.47	8.61
22	5.7	175	19	5.07	7.55
23	4.3	174	19	3.77	5.52
24	6	174	19	5.43	8.23
25	5.8	175	19	5.18	7.76
26	5	173	19	4.36	6.41
27	5.4	171	19	4.77	7.14
28	5.2	125	19	5.54	8.66
29	5.8	127	19	6.12	9.69
30	5.6	127	19	5.89	9.29
31	5	175	19	4.34	6.33
32	5.4	175	19	4.74	6.98
33	4.3	175	19	3.77	5.48
34	5.1	172	19	4.46	6.60
35	5.9	125	19	6.31	9.98
36	4	175	19	3.57	5.23
37	6	125	19	6.43	10.20
38	5.6	127	19	5.89	9.29
39	6	175	19	5.42	8.19
40	5.3	126	19	5.61	8.78

Table 8. Cont.

Sr. No.	WFS	TS	V	Bead Height	Bead Width
41	5.3	127	19	5.57	8.74
42	5.8	175	19	5.18	7.76
43	5.7	175	19	5.07	7.55
44	5.6	125	19	5.96	9.37
45	5.6	171	19	4.98	7.52
46	4.5	175	19	3.92	5.69
47	5.1	175	19	4.44	6.48
48	5.6	175	19	4.95	7.35
49	4.6	172	19	4.02	5.92
50	5.4	174	19	4.74	7.02

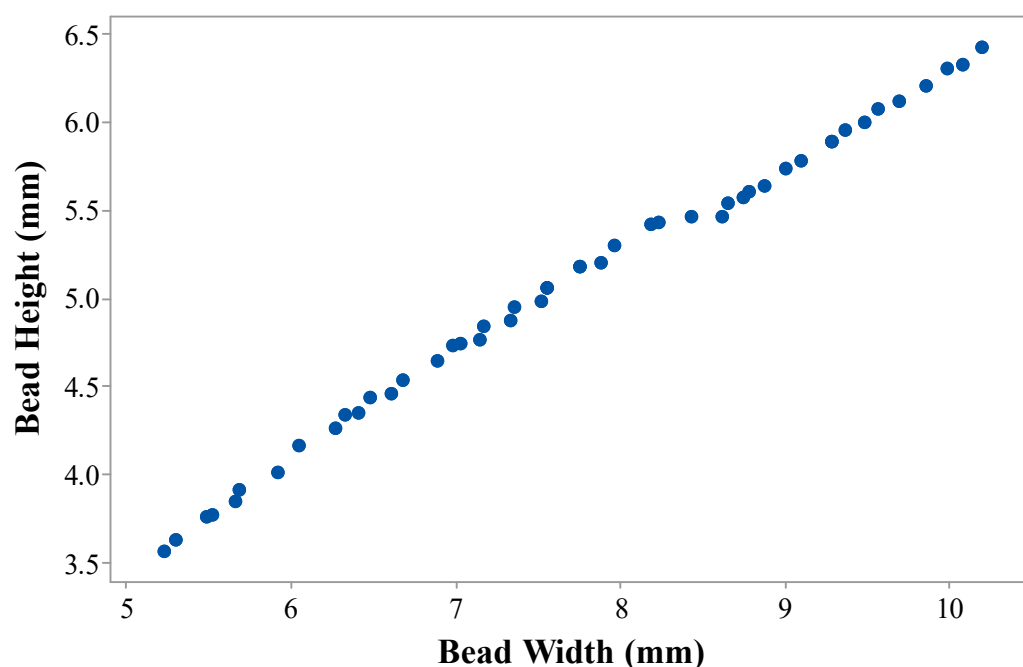


Figure 9. Pareto graph for bead height vs. bead width.

Both of the responses of bead geometries, i.e., bead width and bead height, play a key role in the fabrication of multi-layer thin-walled structures. By considering the equal importance of both responses, a case study consisting of equal weights of BW and BH during the optimization was selected for the fabrication of a multi-layer structure. As per Table 7, the selected case study yielded the optimized values of bead height and bead width of 5.01 mm and 7.81 mm, respectively, at a WFS of 5.50 m/min, TS of 141 mm/min, and voltage of 19 V. Initially, a single-layered trial was conducted for the predicted WAAM variables. Actual experimental values yielded an error of 3.47% and 3.72% for bead height and bead width, respectively, with their BH value of 5.17 mm and BW value of 7.53 mm. An acceptable error between the predicted results and the actual results showed the suitability of the parameters for the fabrication of a multi-layer structure. A multi-layer structure fabricated at the optimal parameter setting of WAAM variables can be seen in Figure 10. Figure 11a,b depict the length and height of the fabricated multi-layered structure which were found to be 130 mm and 60 mm, respectively. A uniform bead-on-bead deposition was observed for the multi-layered structure. Between the two successive layers of the multi-layer structure, a cooling time of 15 s was preferred for the solidification of the next

layer of deposition [46]. Some residual stresses were also released due to the provided cooling time [23]. The multi-layered structure obtained at the optimized parameter was found to be free from disbonding, and seamless fusion was detected between the obtained layers of the structure. Very few lumps of metal were observed on the extreme sides of the deposition. However, the start and stop are always scrapped in the post processing. Thus, the current study successfully demonstrated the necessity of a parametric study for obtaining the desired quality of thin multi-layered structures by employing the GMAW-based WAAM process on an SS 316L substrate. The authors believe that the present study will be beneficial for industrial applications for the fabrication of multi-layer structures.



Figure 10. Multi-layered structure from WAAM process on SS 316L substrate.



(a)

(b)

Figure 11. Multi-layered structure showing (a) length and (b) width on SS 316L substrate.

4. Conclusions

In the present study, GMAW-based WAAM was employed to perform bead-on-plate trials on an SS 316L substrate by considering the TS, WFS, and V as design variables, while BH and BW were considered as responses. The HTS algorithm was employed to obtain the optimal combinations of design variables by considering single- and multi-objective optimization of BH and BW. The obtained results and key findings are summarized below:

- Non-linear regression equations were generated to establish relationships among the WAAM design variables and responses (BH and BW) by integrating the BBD approach of RSM.
- For both responses of bead width and bead height, ANOVA showed the statistical significance of the quadratic model for regression, linear, square, and interaction model terms. Non-significance of the lack of fit specified the acceptability and fitness of the model for bead width and bead height. An R^2 value adjacent to one showed adequacy and acceptability through the validation results of the ANOVA test.
- WFS was the highest contributor affecting the BW response followed by V and TS. WFS was the highest contributor affecting the BH response followed by TS and V. A normal probability plot of residuals successfully validated the ANOVA test results for both bead width and bead height.
- Both of the responses of bead width and bead height of single-layer deposition increased with an increase in WFS and V and a drop in TS. However, opposing objectives are required for the response.
- The HTS approach was used as an optimization technique for a set of optimal levels of both responses. The single-objective optimization result showed a maximum bead height and minimum bead width of 6.72 mm and 3.72 mm, respectively.
- Multiple case studies and Pareto optimal points were conducted by considering the requirement of industrial users for the fabrication of different types of multi-layered structures. All case studies were validated by performing single-layer deposition trials. An error of less than 6% between the predicted results and the actual results showed good agreement between the bead geometry and WAAM variables.
- In the present work, a multi-layer structure was fabricated with the consideration of equal weights of BW and BH during the optimization. The selected case study yielded optimized values of bead height and bead width of 5.01 mm and 7.81 mm, respectively, at a WFS of 5.50 m/min, TS of 141 mm/min, and voltage of 19 V. The multi-layer structure fabricated at the optimal parameter setting of WAAM variables showed a uniform bead-on-bead deposition for the multi-layered structure. The multi-layered structure obtained at the optimized parameter was found to be free from disbonding, and seamless fusion was detected between the obtained layers of the structure.
- Thus, the current study successfully demonstrated the necessity of a parametric study for obtaining the desired quality of thin multi-layered structures by employing the GMAW-based WAAM process on an SS 316L substrate. The authors believe that the present study will be beneficial for industrial applications for the fabrication of multi-layer structures.

Author Contributions: Conceptualization, R.C., H.P., J.V.; methodology, R.C., H.P., J.V., V.K.P.; software, V.K.P.; validation, R.C., J.V.; formal analysis, J.V., V.K.P.; investigation, J.V., R.C.; resources, R.C., H.P., J.V.; data curation, J.V., V.K.P.; writing—original draft preparation, R.C., H.P.; writing—review and editing, J.V., V.K.P.; visualization, R.C., J.V.; supervision, J.V. All authors have read and agreed to the published version of the manuscript.

Funding: The authors would like to thank ORSP, PDEU, for sponsoring the research project in the SRP scheme via project number ORSP/R&D/SRP/2021/010.

Institutional Review Board Statement: Not applicable.

Informed Consent Statement: Not applicable.

Data Availability Statement: Data presented in this study are available in this article.

Acknowledgments: The authors would like to acknowledge the project funded by the Department of Science and Technology (DST), India (SR/FTP/ETA-19/08), for providing a GMAW machining setup.

Conflicts of Interest: The authors declare no conflict of interest.

References

1. Korkmaz, M.E.; Waqar, S.; Garcia-Collado, A.; Gupta, M.K.; Krolczyk, G.M. A technical overview of metallic parts in hybrid additive manufacturing industry. *J. Mater. Res. Technol.* **2022**, *18*, 384–395. [[CrossRef](#)]
2. Svetlizky, D.; Das, M.; Zheng, B.; Vyatskikh, A.L.; Bose, S.; Bandyopadhyay, A.; Schoenung, J.M.; Lavernia, E.J.; Eliaz, N. Directed energy deposition (DED) additive manufacturing: Physical characteristics, defects, challenges and applications. *Mater. Today* **2021**, *49*, 271–295. [[CrossRef](#)]
3. Moeinfar, K.; Khodabakhshi, F.; Kashani-bozorg, S.; Mohammadi, M.; Gerlich, A. A review on metallurgical aspects of laser additive manufacturing (LAM): Stainless steels, nickel superalloys, and titanium alloys. *J. Mater. Res. Technol.* **2021**, *16*, 1029–1068. [[CrossRef](#)]
4. Dinovitzer, M.; Chen, X.; Laliberte, J.; Huang, X.; Frei, H. Effect of wire and arc additive manufacturing (WAAM) process parameters on bead geometry and microstructure. *Addit. Manuf.* **2019**, *26*, 138–146. [[CrossRef](#)]
5. Knapp, G.; Mukherjee, T.; Zuback, J.; Wei, H.; Palmer, T.; De, A.; DebRoy, T. Building blocks for a digital twin of additive manufacturing. *Acta Mater.* **2017**, *135*, 390–399. [[CrossRef](#)]
6. Popov, V.V.; Fleisher, A. Hybrid additive manufacturing of steels and alloys. *Manuf. Rev.* **2020**, *7*, 6. [[CrossRef](#)]
7. Willy, H.J.; Li, X.; Chen, Z.; Herng, T.S.; Chang, S.; Ong, C.Y.A.; Li, C.; Ding, J. Model of laser energy absorption adjusted to optical measurements with effective use in finite element simulation of selective laser melting. *Mater. Des.* **2018**, *157*, 24–34. [[CrossRef](#)]
8. Wang, L.; Xue, J.; Wang, Q. Correlation between arc mode, microstructure, and mechanical properties during wire arc additive manufacturing of 316L stainless steel. *Mater. Sci. Eng. A* **2019**, *751*, 183–190. [[CrossRef](#)]
9. Ke, W.; Oliveira, J.; Cong, B.; Ao, S.; Qi, Z.; Peng, B.; Zeng, Z. Multi-layer deposition mechanism in ultra high-frequency pulsed wire arc additive manufacturing (WAAM) of NiTi shape memory alloys. *Addit. Manuf.* **2022**, *50*, 102513. [[CrossRef](#)]
10. Cui, J.; Yuan, L.; Commins, P.; He, F.; Wang, J.; Pan, Z. WAAM process for metal block structure parts based on mixed heat input. *Int. J. Adv. Manuf. Technol.* **2021**, *113*, 503–521. [[CrossRef](#)]
11. Ding, D.; Pan, Z.; Cuiuri, D.; Li, H. Wire-feed additive manufacturing of metal components: Technologies, developments and future interests. *Int. J. Adv. Manuf. Technol.* **2015**, *81*, 465–481. [[CrossRef](#)]
12. Xiong, J.; Li, Y.; Li, R.; Yin, Z. Influences of process parameters on surface roughness of multi-layer single-pass thin-walled parts in GMAW-based additive manufacturing. *J. Mater. Process. Technol.* **2018**, *252*, 128–136. [[CrossRef](#)]
13. Yang, K.; Wang, F.; Duan, D.; Zhang, T.; Luo, C.; Cressault, Y.; Yu, Z.; Yang, L.; Li, H. Experimental Investigation of Integrated Circular Triple-Wire Pulse GMAW of Q960E High-Strength Steel for Construction Machinery. *Materials* **2021**, *14*, 375. [[CrossRef](#)]
14. Zhang, J.; Zhang, X.; Wang, X.; Ding, J.; Traoré, Y.; Paddea, S.; Williams, S. Crack path selection at the interface of wrought and wire+ arc additive manufactured Ti–6Al–4V. *Mater. Des.* **2016**, *104*, 365–375. [[CrossRef](#)]
15. Srivastava, S.; Garg, R. Process parameter optimization of gas metal arc welding on IS: 2062 mild steel using response surface methodology. *J. Manuf. Process.* **2017**, *25*, 296–305. [[CrossRef](#)]
16. Mai, D.S.; Doan, T.K.; Paris, H. Wire and arc additive manufacturing of 308L stainless steel components: Optimization of processing parameters and material properties. *Eng. Sci. Technol. Int. J.* **2021**, *24*, 1015–1026.
17. Choudhury, S.S.; Marya, S.K.; Amirthalingam, M. Improving arc stability during wire arc additive manufacturing of thin-walled titanium components. *J. Manuf. Process.* **2021**, *66*, 53–69. [[CrossRef](#)]
18. Wu, B.; Pan, Z.; Ding, D.; Cuiuri, D.; Li, H.; Xu, J.; Norrish, J. A review of the wire arc additive manufacturing of metals: Properties, defects and quality improvement. *J. Manuf. Process.* **2018**, *35*, 127–139. [[CrossRef](#)]
19. Zhao, Y.-t.; Li, W.-g.; Liu, A. Optimization of geometry quality model for wire and arc additive manufacture based on adaptive multi-objective grey wolf algorithm. *Soft Comput.* **2020**, *24*, 17401–17416. [[CrossRef](#)]
20. Vora, J.; Patel, V.K.; Srinivasan, S.; Chaudhari, R.; Pimenov, D.Y.; Giasin, K.; Sharma, S. Optimization of activated tungsten inert gas welding process parameters using heat transfer search algorithm: With experimental validation using case studies. *Metals* **2021**, *11*, 981. [[CrossRef](#)]
21. Vora, J.; Chaudhari, R.; Patel, C.; Pimenov, D.Y.; Patel, V.K.; Giasin, K.; Sharma, S. Experimental Investigations and Pareto Optimization of Fiber Laser Cutting Process of Ti6Al4V. *Metals* **2021**, *11*, 1461. [[CrossRef](#)]
22. Fuse, K.; Chaudhari, R.; Vora, J.; Patel, V.K.; de Lacalle, L.N.L. Multi-Response Optimization of Abrasive Waterjet Machining of Ti6Al4V Using Integrated Approach of Utilized Heat Transfer Search Algorithm and RSM. *Materials* **2021**, *14*, 7746. [[CrossRef](#)] [[PubMed](#)]
23. Kumar, V.; Mandal, A.; Das, A.K.; Kumar, S. Parametric study and characterization of wire arc additive manufactured steel structures. *Int. J. Adv. Manuf. Technol.* **2021**, *115*, 1723–1733. [[CrossRef](#)]
24. Yuan, L.; Ding, D.; Pan, Z.; Yu, Z.; Wu, B.; van Duin, S.; Li, H.; Li, W. Application of multidirectional robotic wire arc additive manufacturing process for the fabrication of complex metallic parts. *IEEE Trans. Ind. Inform.* **2019**, *16*, 454–464. [[CrossRef](#)]
25. Kannan, T.; Murugan, N. Effect of flux cored arc welding process parameters on duplex stainless steel clad quality. *J. Mater. Process. Technol.* **2006**, *176*, 230–239. [[CrossRef](#)]
26. Teixeira, F.R.; Scotti, F.M.; Vilarinho, L.O.; da Mota, C.A.M.; Scotti, A. Transferability of the working envelope approach for parameter selection and optimization in thin wall WAAM. *Int. J. Adv. Manuf. Technol.* **2022**, *119*, 969–989. [[CrossRef](#)]
27. Cadiou, S.; Courtois, M.; Carin, M.; Berckmans, W. 3D heat transfer, fluid flow and electromagnetic model for cold metal transfer wire arc additive manufacturing (Cmt-Waam). *Addit. Manuf.* **2020**, *36*, 101541. [[CrossRef](#)]

28. Vora, J.; Parikh, N.; Chaudhari, R.; Patel, V.K.; Paramar, H.; Pimenov, D.Y.; Giasin, K. Optimization of Bead Morphology for GMAW-Based Wire-Arc Additive Manufacturing of 2.25 Cr-1.0 Mo Steel Using Metal-Cored Wires. *Appl. Sci.* **2022**, *12*, 5060. [[CrossRef](#)]
29. Senthil, T.; Babu, S.R.; Puviyarasan, M.; Dhinakaran, V. Mechanical and microstructural characterization of functionally graded Inconel 825-SS316L fabricated using wire arc additive manufacturing. *J. Mater. Res. Technol.* **2021**, *15*, 661–669. [[CrossRef](#)]
30. Khidhir, G.I.; Baban, S.A. Efficiency of dissimilar friction welded 1045 medium carbon steel and 316L austenitic stainless steel joints. *J. Mater. Res. Technol.* **2019**, *8*, 1926–1932. [[CrossRef](#)]
31. Vieira, D.; Siqueira, R.; Carvalho, S.; Lima, M. Effect of the initial substrate temperature on heat transfer and related phenomena in austenitic stainless steel parts fabricated by additive manufacturing using direct energy deposition. *J. Mater. Res. Technol.* **2022**, *18*, 5267–5279.
32. Saboori, A.; Aversa, A.; Marchese, G.; Biamino, S.; Lombardi, M.; Fino, P. Microstructure and mechanical properties of AISI 316L produced by directed energy deposition-based additive manufacturing: A review. *Appl. Sci.* **2020**, *10*, 3310. [[CrossRef](#)]
33. Ferreira, S.C.; Bruns, R.; Ferreira, H.S.; Matos, G.D.; David, J.; Brandão, G.; da Silva, E.P.; Portugal, L.; Dos Reis, P.; Souza, A. Box-Behnken design: An alternative for the optimization of analytical methods. *Anal. Chim. Acta* **2007**, *597*, 179–186. [[CrossRef](#)] [[PubMed](#)]
34. Wu, W.; Xue, J.; Xu, W.; Lin, H.; Tang, H.; Yao, P. Parameters optimization of auxiliary gas process for double-wire SS316L stainless steel arc additive manufacturing. *Metals* **2021**, *11*, 190. [[CrossRef](#)]
35. Patel, V.K.; Savsani, V.J. Heat transfer search (HTS): A novel optimization algorithm. *Inf. Sci.* **2015**, *324*, 217–246. [[CrossRef](#)]
36. Chaudhari, R.; Vora, J.J.; Mani Prabu, S.; Palani, I.; Patel, V.K.; Parikh, D.; de Lacalle, L.N.L. Multi-response optimization of WEDM process parameters for machining of superelastic nitinol shape-memory alloy using a heat-transfer search algorithm. *Materials* **2019**, *12*, 1277. [[CrossRef](#)]
37. Raja, B.D.; Patel, V.; Jhala, R.L. Thermal design and optimization of fin-and-tube heat exchanger using heat transfer search algorithm. *Therm. Sci. Eng. Prog.* **2017**, *4*, 45–57. [[CrossRef](#)]
38. Fuchs, C.; Baier, D.; Semm, T.; Zaeh, M.F. Determining the machining allowance for WAAM parts. *Prod. Eng.* **2020**, *14*, 629–637. [[CrossRef](#)]
39. Vora, J.; Khanna, S.; Chaudhari, R.; Patel, V.K.; Paneliya, S.; Pimenov, D.Y.; Giasin, K.; Prakash, C. Machining parameter optimization and experimental investigations of nano-graphene mixed electrical discharge machining of nitinol shape memory alloy. *J. Mater. Res. Technol.* **2022**, *19*, 653–668. [[CrossRef](#)]
40. Al-Amin, M.; Abdul-Rani, A.M.; Ahmed, R.; Shahid, M.U.; Zohura, F.T.; Rani, M.D.B.A. Multi-objective optimization of process variables for MWCNT-added electro-discharge machining of 316L steel. *Int. J. Adv. Manuf. Technol.* **2021**, *115*, 179–198. [[CrossRef](#)]
41. Ghazvinloo, H.; Honarbakhsh-Raouf, A. Numerical Modeling of Heat-Affected Zone in the GMAW Process. *Mater. Sci.* **2021**, *56*, 807–813. [[CrossRef](#)]
42. Panda, B.; Shankhwar, K.; Garg, A.; Savalani, M. Evaluation of genetic programming-based models for simulating bead dimensions in wire and arc additive manufacturing. *J. Intell. Manuf.* **2019**, *30*, 809–820. [[CrossRef](#)]
43. Pan, Z.; Ding, D.; Wu, B.; Cuiuri, D.; Li, H.; Norrish, J. Arc welding processes for additive manufacturing: A review. *Trans. Intell. Weld. Manuf.* **2018**, *1*, 3–24.
44. Yehorov, Y.; da Silva, L.J.; Scotti, A. Balancing WAAM production costs and wall surface quality through parameter selection: A case study of an Al-Mg5 alloy multilayer-non-oscillated single pass wall. *J. Manuf. Mater. Process.* **2019**, *3*, 32. [[CrossRef](#)]
45. Zhou, Y.; Lin, X.; Kang, N.; Huang, W.; Wang, J.; Wang, Z. Influence of travel speed on microstructure and mechanical properties of wire+ arc additively manufactured 2219 aluminum alloy. *J. Mater. Sci. Technol.* **2020**, *37*, 143–153. [[CrossRef](#)]
46. Lehmann, T.; Jain, A.; Jain, Y.; Stainer, H.; Wolfe, T.; Henein, H.; Qureshi, A.J. Concurrent geometry-and material-based process identification and optimization for robotic CMT-based wire arc additive manufacturing. *Mater. Des.* **2020**, *194*, 108841. [[CrossRef](#)]